O and N co-doped porous carbon derived from crop wastes for high-stability all-solid-state symmetric supercapacitor

Fengyu Wu[a#], Xue Ren[a#], Fenyang Tian[a], Guanghui Han[a], Jie Sheng[b], Yongsheng Yu[a*], Yequn Liu[c*] and Weiwei Yang[a*]

[a]MIIT Key Laboratory of Critical Materials Technology for New Energy Conversion and Storage, School of Chemistry and Chemical Engineering, Harbin Institute of Technology, Harbin, 150001, China

[b]Laboratory for Space Environment and Physical Science, Research Center of Basic Space Science, Harbin Institute of Technology, Harbin 150001, China

[c]Analytical Instrumentation Center, State Key Laboratory of Coal Conversion, Institute of Coal Chemistry, Chinese Academy of Sciences, Taiyuan, Shanxi 030001, China

# These authors contributed equally.

*Corresponding authors.

E-mail addresses: yangww@hit.edu.cn (W. Yang), liuyequn@sxicc.ac.cn (Y. Liu), ysyu@hit.edu.cn (Y. Yu).

Materials

SP was obtained from the soybean straw purchased from Suihua City, Heilongjiang Province. Potassium hydroxide (KOH, 97%) was provided by Aladdin Reagent Co., LTD. Anhydrous ethanol (CH_3CH_2OH, AR) and Hydrochloric acid (HCl, 12 M) were supplied by Sinopharm Chemical Reagent Co. LTD. Polyvinyl alcohol (PVA-117) was provided by Aladdin Reagent Co., LTD. All reagents were used without further purification.

Material characterization

The morphology of samples was recorded on field-emission scanning electron microscopy (FE-SEM, Supra 55, Zeiss). Transmission electron microscopy (TEM) and high-resolution transmission electron microscopy (HRTEM) images were obtained using JEM-1400 and JEM-2100. X-ray diffraction (XRD) patterns were tested on a PAN analytical X'Pert Powder with Cu Kα radiation (λ = 1.5418 Å). The Raman spectra were evaluated using LabRAM HR Evolution with a 532 nm excitation laser. And the X-ray photoelectron spectroscopic (XPS) measurement was recorded on a Thermo ESCALAB 250Xi instrument.

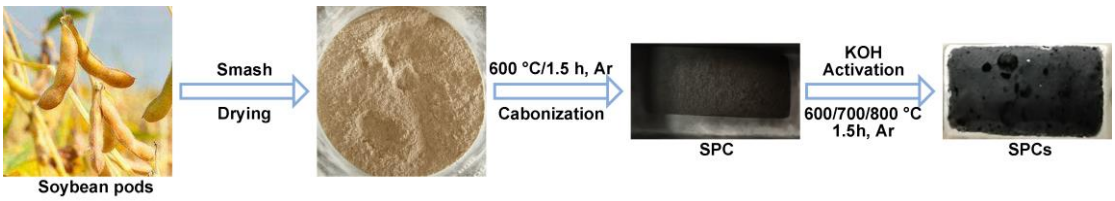

Fig. S1 Preparation process of soybean pod-derived porous carbon.

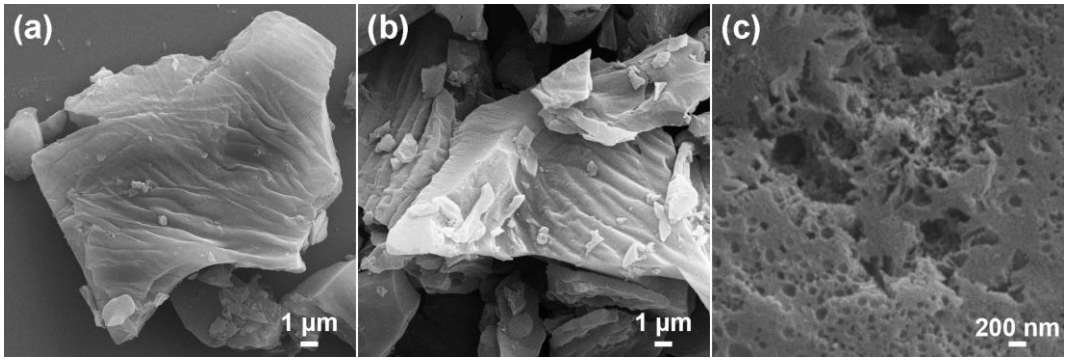

Fig. S2 Morphology characterization of SPC and SPC/700 °C/3. SEM images of (a) SPC, (b, c) SPC/700 °C/3

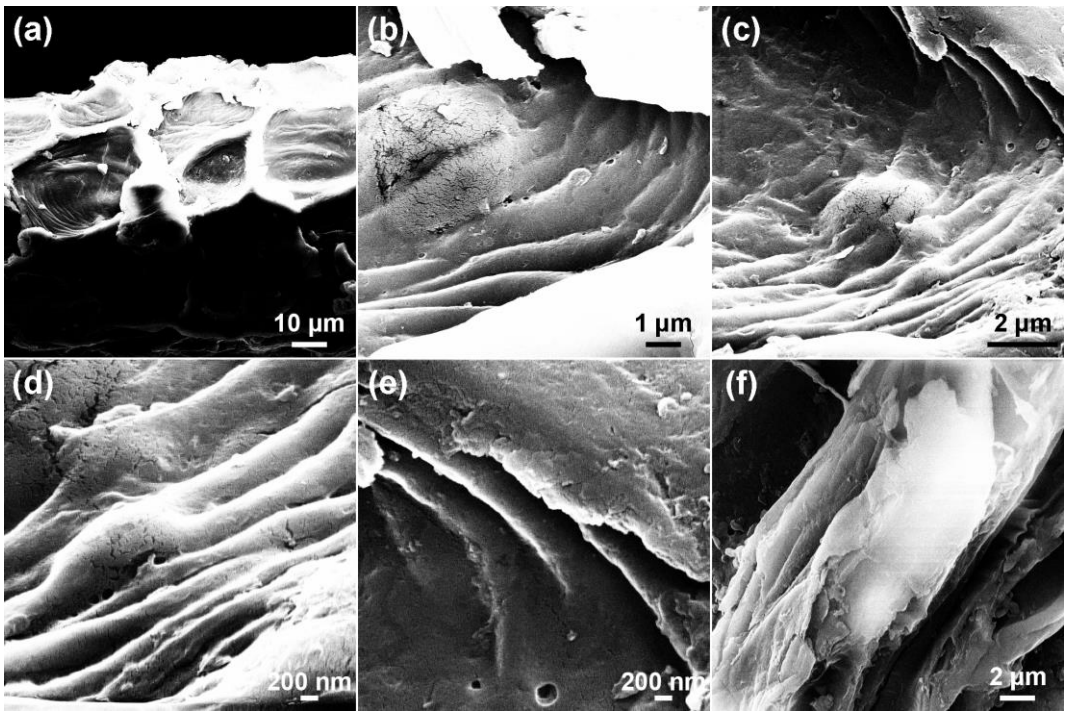

Fig. S3 SEM images of SP.

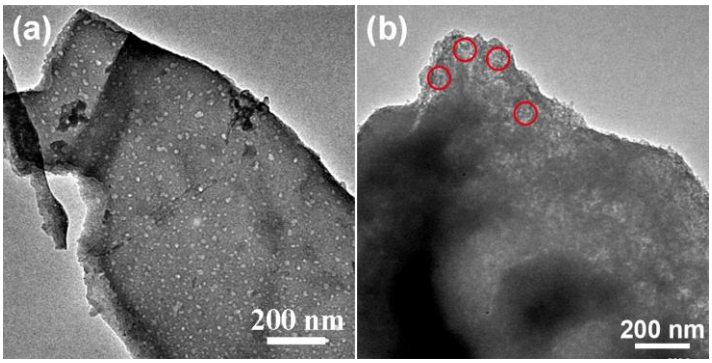

Fig. S4 TEM images of (a) SPC/700°C/1, (b) SPC/700°C/5.

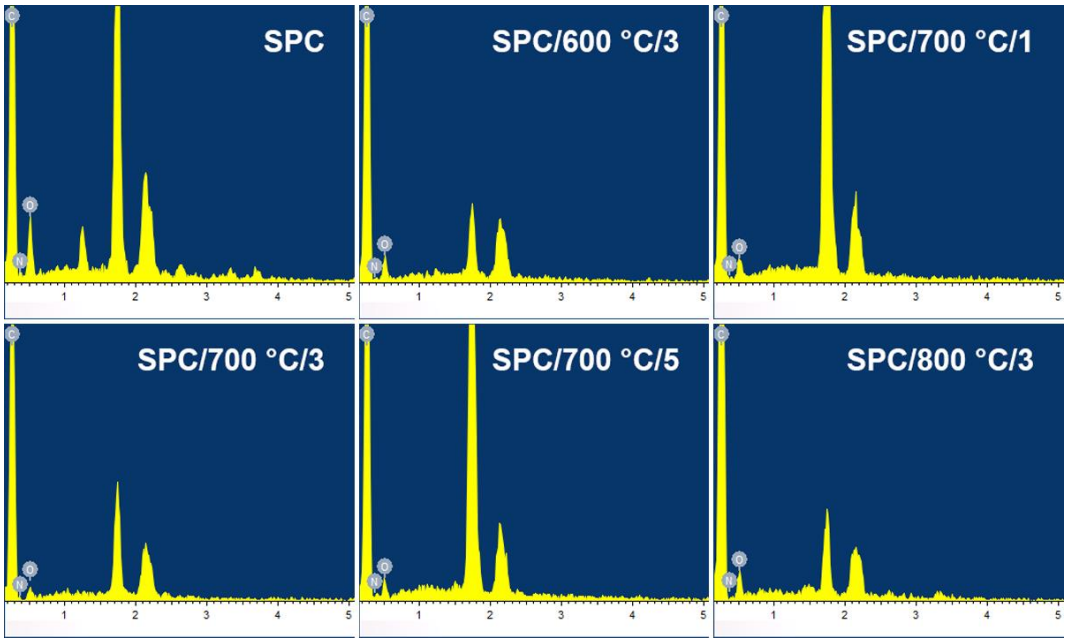

Fig. S5 EDS spectrum of SPCs.

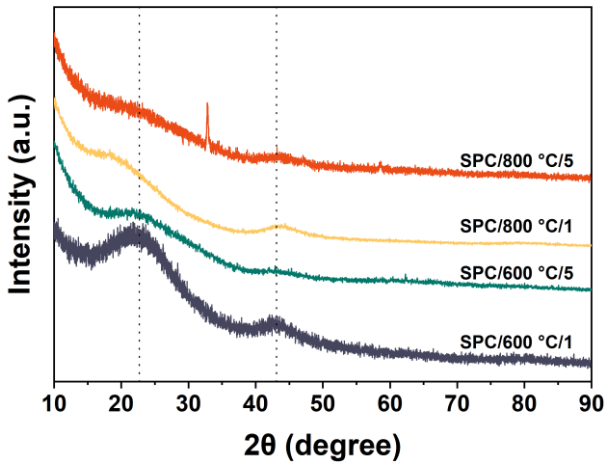

Fig. S6 XRD patterns of SPC/600℃/1, SPC/600℃/5, SPC/800℃/1 and SPC/800℃/5.

Table S1 Surface elemental compositions of SPC and SPC/700 °C/3

Samples	Surface Elemental Analysis, at%			
	C	O	N	Heteroatom
SPC	93.11	5.91	0.98	6.89
SPC/700 °C/3	89.23	9.86	0.91	10.77

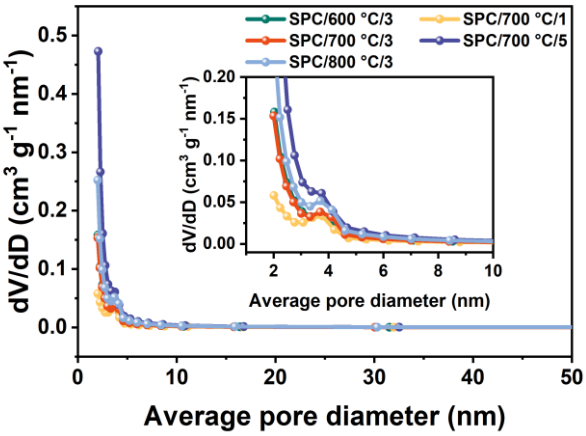

Fig. S7 Mesopore size distribution of SPCs.

Table S2 Pore structure characteristics of SPCS

Samples	S_{BET} (m^2 g^{-1})	V_{total} (cm^3 g^{-1})	D_{aver} (nm)
SPC	9.0721	0.0127	5.5996
SPC/600 °C/3	1805.21	1.0098	2.2375
SPC/700 °C/1	889.228	0.5326	2.3958
SPC/700 °C/3	1807.56	1.0347	2.2897
SPC/700 °C/5	2891.23	1.5607	2.1592
SPC/800 °C/3	2052.52	1.1934	2.3257

The electrochemical performance of Ni foam was tested in the three-electrode system in the 6 M KOH aqueous electrolyte (Fig. S8). And the specific capacitance was calculated to only be 1.05 F g^{-1} at 1 A g^{-1}.

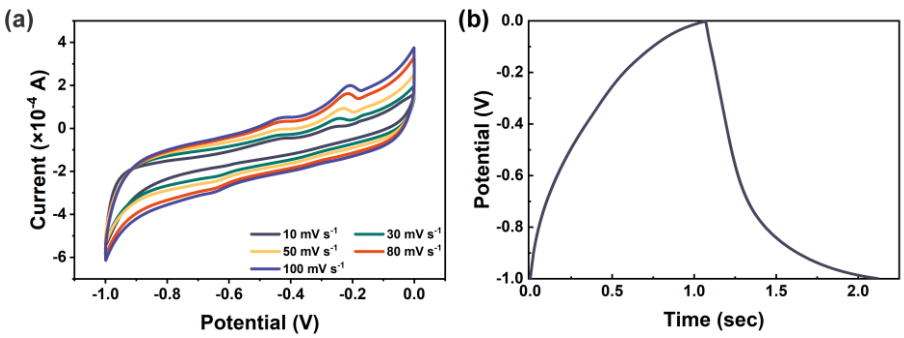

Fig. S8 Electrochemical performance of pure Ni foam measured in a three-electrode system in the 6 M KOH electrolyte. (a) CV curves at 10-100 mV s^{-1}, (b) GCD curves at 1 A g^{-1}.

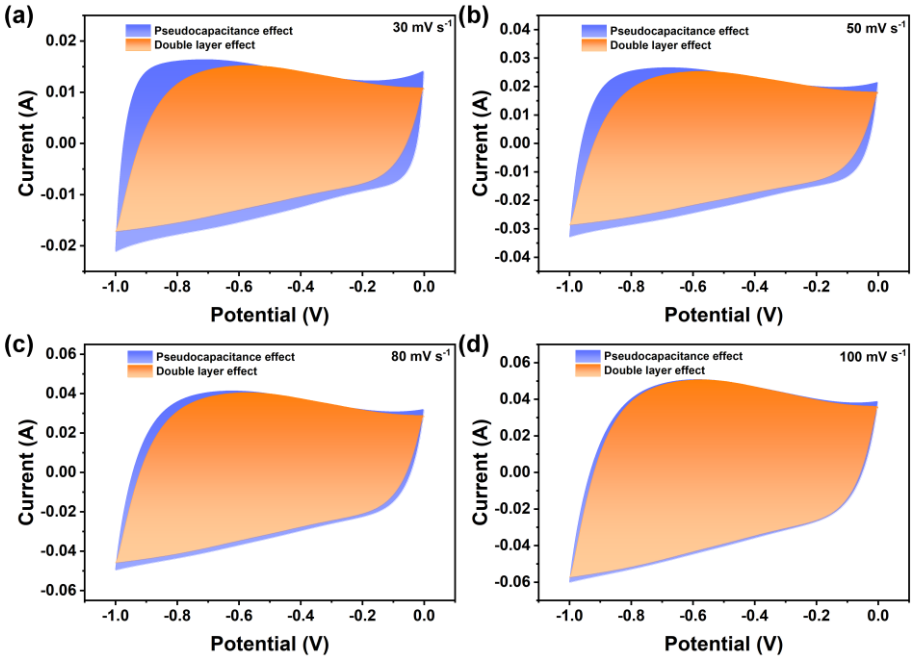

Fig. S9 The schematic diagram of capacitance contribution of SPC/700 °C/3 (a)30 mV s^{-1}, (b)50 mV s^{-1}, (c)80 mV s^{-1}, (d)100 mV s^{-1}.

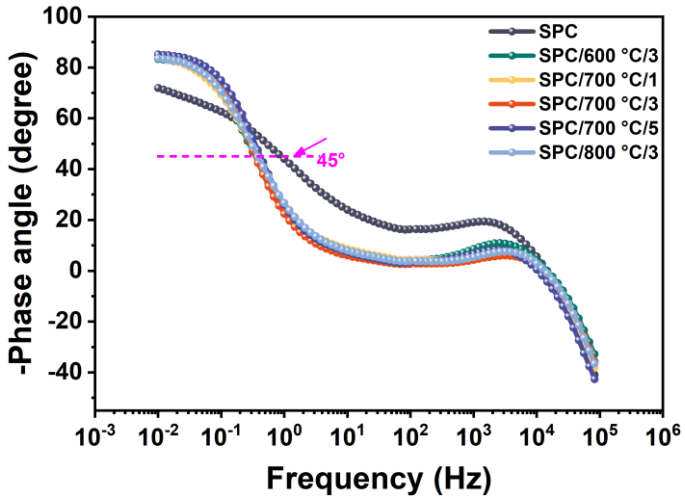

Fig. S10 Bode phase angle plots of SPC and SPCs electrodes.

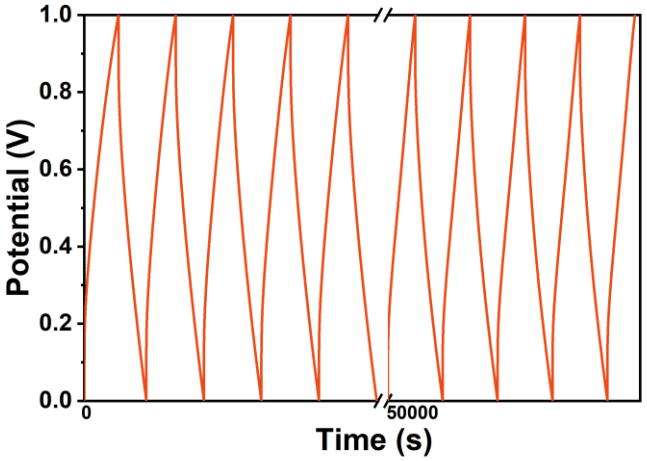

Fig. S11 The GCD curves of the first 5 cycles and the last 5 cycles during the cycle.